HHS Public Access

Author manuscript

Neuron. Author manuscript; available in PMC 2018 April 19.

Published in final edited form as:

Neuron. 2017 April 19; 94(2): 294–303.e4. doi:10.1016/j.neuron.2017.03.024.

Respiratory network stability and modulatory response to substance P require Nalcn

Szu-Ying Yeh[1,6], **Wei-Hsiang Huang**[1,6,#], **Wei Wang**[2,6], **Christopher S. Ward**[2,6], **Eugene S. Chao**[3,6,7], **Zhenyu Wu**[4,6], **Bin Tang**[4,6], **Jianrong Tang**[4,6], **Jenny J. Sun**[3], **Meike Esther van der Heijden**[3,6], **Paul A. Gray**[8,&], **Mingshan Xue**[1,3,6,7], **Russell S. Ray**[1,3], **Dejian Ren**[9], and **Huda Y. Zoghbi**[1,2,3,4,5,6,*]

[1]Program in Developmental Biology, Texas Children's Hospital, Baylor College of Medicine, Houston, Texas 77030, USA

[2]Department of Molecular and Human Genetics, Texas Children's Hospital, Baylor College of Medicine, Houston, Texas 77030, USA

[3]Department of Neuroscience, Texas Children's Hospital, Baylor College of Medicine, Houston, Texas 77030, USA

[4]Department of Pediatrics, Texas Children's Hospital, Baylor College of Medicine, Houston, Texas 77030, USA

[5]Howard Hughes Medical Institute, Texas Children's Hospital, Baylor College of Medicine, Houston, Texas 77030, USA

[6]Jan and Dan Duncan Neurological Research Institute, Texas Children's Hospital, Baylor College of Medicine, Houston, Texas 77030, USA

[7]The Cain Foundation Laboratories at Texas Children's Hospital, Houston, Texas 77030, USA

[8]Department of Anatomy and Neurobiology, Washington University School of Medicine, St. Louis, MO 63110, USA

[9]Department of Biology, University of Pennsylvania, 415 South University Avenue, Philadelphia, PA 19104, USA

SUMMARY

[*]Lead Contact: hzoghbi@bcm.edu.

[#]Present address: Howard Hughes Medical Institute and Department of Biology, Stanford University, Stanford, CA 94305, USA

[&]Present address: Indigo Ag, Inc, Cambridge, MA 02142, USA

AUTHOR CONTRIBUTIONS

S.-Y.Y., W.-H.H., and H.Y.Z. conceived and designed the experiments. P.A.G. provided the critical input to the project. S.-Y.Y., W.-H.H., W.W., C.S.W., E.S.C., Z.W., B.T., J.T., J.J.S., M.X., and R.S.R. performed the experiments. M.E.H. performed UWBP analysis. D.R. assisted in generating the mouse model. S.-Y.Y., W.-H.H., and H.Y.Z. drafted the original manuscript, and all authors assisted in editing the manuscript.

Respiration is a rhythmic activity as well as one that requires responsiveness to internal and external circumstances; both the rhythm and neuromodulatory responses of breathing are controlled by brainstem neurons in the preBötzinger Complex (preBötC) and the retrotrapezoid nucleus (RTN), but the specific ion channels essential to these activities remain to be identified. Because deficiency of *Sodium leak channel, non-selective (Nalcn)* causes lethal apnea in humans and mice, we investigated Nalcn function in these neuronal groups. We found that one-third of mice lacking *Nalcn* in excitatory preBötC neurons died soon after birth; surviving mice developed apneas in adulthood. Interestingly, in both preBötC and RTN neurons, the Nalcn current influences the resting membrane potential, contributes to maintenance of stable network activity, and mediates modulatory responses to the neuropeptide substance P. These findings reveal Nalcn's specific role in both rhythmic stability and responsiveness to neuropeptides within the respiratory network.

INTRODUCTION

Rhythmicity governs many biological functions, on scales ranging from subseconds to months, during both waking and sleeping states. These rhythms must strike a balance between a regular, intrinsic pattern and the ability to respond to changing environmental and physiological conditions. In the case of respiration, neurons in the preBötzinger Complex (preBötC) show characteristics of central pattern generator (CPG) that generates inspiratory movements and is coupled with chemosensory neurons, such as retrotrapezoid nucleus (RTN) (Feldman et al., 2013; Guyenet et al., 2016; Ramirez et al., 2016; Smith et al., 1991; Smith et al., 1989). Specifically, the glutamatergic subpopulation of preBötC neurons generates the inspiratory rhythms essential for breathing (Wang et al., 2014), while the RTN neurons (all of which are glutamatergic) provide rhythmic excitatory drive to the preBötC during early development and during active expiration upon physical exercise (Pagliardini et al., 2011; Thoby-Brisson et al., 2009). Importantly, neurons within the preBötC and RTN are intrinsically active but must also respond to neuromodulatory inputs. For example, subsets of chemosensitive serotonergic neurons within the ventral lateral medulla innervate the RTN and preBötC regions and increase respiratory activity by releasing neuromodulators such as substance P and serotonin (Mulkey et al., 2007; Ptak et al., 2009). The substance P receptor, neurokinin 1 receptor (NK1R), is coupled with voltage-independent cation channels to increase neuronal excitability (Hayes and Del Negro, 2007; Koizumi et al., 2010; Pena and Ramirez, 2004; Ptak et al., 2009). What remains unclear, however, is how the network activity and exogenous inputs are coordinated into a properly responsive respiratory response.

We were interested in identifying ion channels that might participate in rhythm generation, chemosensitivity, or substance P modulation, and decided to investigate the nonselective cation channel *Sodium leak channel, non-selective (Nalcn).* In human, *NALCN* mutations show severe respiratory dysfunction (Chong et al., 2015; Gal et al., 2016). In mice, *Nalcn* deletion cause periodic apnea, depressed respiratory rhythm, and death within the first postnatal day (P0) (Lu et al., 2007). Given that previous pharmacological studies had shown that neurons within the preBötC and RTN express the persistent Na^+ current (I_{NaP}) and the HCN-mediated inward current (I_h) (Del Negro et al., 2002; Thoby-Brisson et al., 2009;

Thoby-Brisson et al., 2000), but had not tested for the Nalcn current, we decided to use a genetic approach to manipulate Nalcn *in vivo* and to evaluate its functions in inspiratory rhythmogenic and chemosensory neurons within the respiratory network.

RESULTS

Respiratory defects in *Nalcn*-null mice originate in the central nervous system

To delete *Nalcn* in specific cells, we first generated mice carrying the loxP-flanked (floxed) *Nalcn* allele ($Nalcn^{flox}$, Fig. S1A). Cre-mediated recombination deletes exons 5 and 6 and introduces a stop codon, leaving the *Nalcn* transcript undetectable, as confirmed by *in situ* hybridization and qPCR (Fig. S1B–C). We verified that the respiratory phenotype of *Nalcn*-null mice originates from the nervous system by deleting *Nalcn* using a $Nestin^{Cre}$ allele ($Nalcn^{NestinCKO}$) (Tronche et al., 1999). All of the $Nalcn^{NestinCKO}$ mice died within 24 hours of birth (Table 1), mimicking the phenotype of *Nalcn*-null animals. This indicates that Nalcn current in the nervous system is essential for neonatal survival.

Nalcn in glutamatergic neurons sustains neonatal respiration

The respiratory network relies on several neurotransmitters, including glutamate, GABA, serotonin, glycine and acetylcholine (Feldman et al., 2013; Hodges et al., 2009; Janczewski et al., 2013). To identify the neuronal subtypes responsible for the respiratory defects in the *Nalcn*-null mice, we deleted *Nalcn* using $Vglut2^{Cre}$ ($Nalcn^{Vglut2CKO}$) (Vong et al., 2011), $Viaat^{Cre}$ ($Nalcn^{ViaatCKO}$) (Chao et al., 2010), $Chat^{Cre}$ ($Nalcn^{ChatCKO}$) (Rossi et al., 2011), $Pet1^{Cre}$ ($Nalcn^{Pet1CKO}$) (Scott et al., 2005) or $GlyT2^{Cre}$ ($Nalcn^{GlyT2CKO}$) (Ishihara et al., 2010) lines, which target glutamatergic, GABAergic, cholinergic, serotonergic, and glycinergic neurons, respectively. Although 13.2% $Nalcn^{ViaatCKO}$ mice died within 24 hours of birth, none of the $Nalcn^{ChatCKO}$, $Nalcn^{Pet1CKO}$, or $Nalcn^{GlyT2CKO}$ mice died (Table 1). On the other hand, all $Nalcn^{Vglut2CKO}$ mice died within 24 hours of birth (Table 1). Therefore, we focused on the glutamatergic preBötC and RTN neurons in the brainstem.

Loss of *Nalcn* in either the preBötC or Atoh1^{+} lineage leads to apneas in awake animals

The conductance and regulation of the Nalcn cation complex depend on the pore-forming subunit (Nalcn itself) and at least two interactors: Unc79 and Unc80 (Lu et al., 2009; Lu et al., 2010). We detected co-localization of *Nalcn*, *Unc79*, and *Unc80* transcripts in the *tdTOMATO* labeled RTN using *Atonal homolog-1*^{Cre} ($Atoh1^{Cre}$) (Yang et al., 2010) at P0 (Fig. S2A). This suggests that the RTN co-expresses components of a functional Nalcn complex. The *Paired like homeobox 2b* (*Phox2b*)-expressing progenitors in the embryonic hindbrain give rise to the glutamatergic RTN neurons (Dubreuil et al., 2009), which require Atoh1 to migrate ventrally toward the facial nucleus (VII) and connect with neurons in the preBötC (Huang et al., 2012; Ruffault et al., 2015). We confirmed our *in situ* hybridization data by fluorescence-activated cell sorting of RTN neurons using the *Atoh1-EGFP* line (Rose et al., 2009) (Fig. S2B–E). Similarly, *Nalcn*, *Unc79*, and *Unc80*, are co-expressed in the genetically labeled glutamatergic neurons within the preBötC area ($tdTOMATO^{+}$) using *Developing brain homeobox protein 1*^{Cre} ($Dbx1^{Cre}$) (Bielle et al., 2005) at P0 (Fig. S2A).

Within the preBötC region, respiratory glutamatergic neurons derive from progenitors expressing *Dbx1* and are critical for respiratory rhythm generation and motor output. (Bouvier et al., 2010; Gray et al., 2010; Picardo et al., 2013; Revill et al., 2015; Wang et al., 2014). Thus, we deleted *Nalcn* in glutamatergic preBötC neurons using the $Dbx1^{Cre}$ line ($Nalcn^{Dbx1CKO}$) and in the RTN using either $Phox2b^{Cre}$ ($Nalcn^{Phox2bCKO}$) (Scott et al., 2011) or $Atoh1^{Cre}$ lines ($Nalcn^{Atoh1CKO}$).

To our surprise, none of the $Nalcn^{Phox2bCKO}$ or $Nalcn^{Atoh1CKO}$ newborns showed neonatal lethality (Table 1), but 33% of the $Nalcn^{Dbx1CKO}$ mice died within 24 hours of birth (Table 1). We performed neonatal head-out pneumotachography to determine whether the perinatal death of $Nalcn^{Dbx1CKO}$ mice was due to respiratory deficits. 28.6% of the $Nalcn^{Dbx1CKO}$ newborns (Fig. 1A, green) showed a significantly greater frequency of apnea than the other newborns, consistent with the lethality rate. One possible explanation for the survival of the $Nalcn^{Dbx1CKO}$ newborns is the excitatory drive from the RTN neurons (Jacquin et al., 1996). However, deleting *Nalcn* from the preBötC and RTN ($Nalcn^{DCKO}$) does not cause additional lethality in mice (Table 1), suggesting that the surviving $Nalcn^{Dbx1CKO}$ newborns might receive compensatory respiratory activity from other $Vglut2^{+}$ neurons.

To determine whether loss of *Nalcn* in the RTN or preBötC affects the responses to hypoxia and hypercapnia in freely-moving adult animals, we used unrestrained whole-body plethysmography (UWBP) to monitor the respiration of 7-week-old $Nalcn^{Phox2bCKO}$, $Nalcn^{Atoh1CKO}$, and $Nalcn^{Dbx1CKO}$ mice. The respiratory rate during exposure to fresh air, hypercapnic (5% CO_2), or hypoxic conditions (10% O_2) was indistinguishable among $Nalcn^{Phox2bCKO}$ (data not shown), $Nalcn^{Atoh1CKO}$, $Nalcn^{Dbx1CKO}$ and control mice, but $Nalcn^{Dbx1CKO}$ mice had longer inspiratory time (Fig. S3A), suggesting that removing *Nalcn* from the RTN and preBötC did not impair breathing frequency or chemoreflexes, while loss of *Nalcn* in preBötC led to disturbed respiratory patterns *in vivo*.

Interestingly, $Nalcn^{Atoh1CKO}$ and $Nalcn^{Dbx1CKO}$ but not $Nalcn^{Phox2bCKO}$ mice showed increased apnea frequency compared to heterozygous and $Nalcn^{flox/flox}$ groups (Fig. 1B–D and S3A–C). Blood gas measurements showed no difference in blood CO_2 levels (Table S1), ruling out disturbance of systematic CO_2 homeostasis. To determine whether the apnea in $Nalcn^{Atoh1CKO}$ mice was due to the lack of *Nalcn* expression in $Atoh1^{+}$ neurons within the pons, we deleted *Nalcn* using $En1^{Cre}$ ($Nalcn^{En1CKO}$) (Kimmel et al., 2000). $Nalcn^{En1CKO}$ mice survived at birth (Table 1) but showed a significantly greater frequency of apnea at 7 weeks (Fig. 1E and S3A). These results indicate that preBötC neurons and Atoh1-dependent neurons, likely from the rhombic lip lineages in the pons, require Nalcn to maintain proper respiration. Furthermore, the expression of Nalcn in the preBötC is critical for neonatal respiration.

PreBötC and RTN neurons require Nalcn conductance for proper rhythm generation

To determine whether Nalcn is important for the biophysical activities of the RTN and preBötC network, we used the patch-clamp technique to assess the biophysical properties of labeled RTN and preBötC network from which we had deleted *Nalcn* using a fluorescent reporter ($Rosa^{LSL\text{-}tdTOMATO}$) (Madisen et al., 2010) (Fig. 2A and 2B). We compared $Nalcn^{Atoh1CKO}$ and $Nalcn^{Dbx1CKO}$ mice to *Nalcn* heterozygous littermates based on the

mating strategy (*Atoh1*^{Cre}; *Nalcn*$^{flox/+}$ x *Nalcn*$^{flox/flox}$; *Rosa*$^{LSL\text{-}tdTOMATO/LSL\text{-}tdTOMATO}$ and *Dbx1*^{Cre}; *Nalcn*$^{flox/+}$ x *Nalcn*$^{flox/flox}$; *Rosa*$^{LSL\text{-}tdTOMATO/LSL\text{-}tdTOMATO}$).

RTN neurons lacking *Nalcn* showed hyperpolarized resting membrane potential (Fig. 2C and Table S2A), a 49% reduction in spontaneous spike frequency (Fig. 2D–E and Table S2A), and a 39% and 23% increase in input resistance and holding current, respectively (Table S2A). Similarly, preBötC neurons lacking *Nalcn* had a hyperpolarized resting membrane potential (Fig. 2F and Table S2B), a 38% reduction in inspiratory neuronal bursting frequency (Fig. 2G–H and Table S2B), a 20% decrease in capacitance, and a 24% and 21% increase in input resistance and holding current, respectively (Table S2B). There was a 47% reduction in network rhythmicity (Fig. 2G′–H′ and Table S2B). We also measured the steady-state current-voltage (*I–V*) relationship from the labeled RTN and preBötC neurons, and loss of *Nalcn* resulted in lower inward current in both populations compared with control cells (Fig. 2I and 2J), consistent with previous observations in the hippocampal and RTN neurons (Lu et al., 2007; Shi et al., 2016). The Nalcn current clearly contributes to the resting membrane potential and the rhythmic activity of the RTN and preBötC neurons.

Modulatory response to substance P in RTN and preBötC requires Nalcn

Substance P has been shown to enhance both RTN firing frequency and the resulting respiratory motor outputs (Mulkey et al., 2007). Moreover, in the hippocampus and ventral tegmental areas, substance P binds to NK1R and mediates slow excitation by activating the Nalcn complex (Lu et al., 2009). To determine whether substance P-mediated slow excitation in the RTN network is Nalcn-dependent, we administrated substance P to brainstem slices containing the RTN. Upon loss of *Nalcn*, the RTN showed a diminished response to substance P (Fig. 2D–E and Table S2A); this is consistent with a recent report that Nalcn contributes to the substance P-mediated membrane conductance in the RTN network (Shi et al., 2016).

It was previously shown that a substance P-mediated, tetrodotoxin (TTX)-resistant low-threshold sodium current modulates neuronal excitability of preBötC (Hayes and Del Negro, 2007; Pena and Ramirez, 2004). We found that deleting *Nalcn* from glutamatergic preBötC neurons reduced neuronal modulatory response to substance P and lowered bursting frequency compared to control neurons (Fig. 2G–H and Table S2B), as well as network response to substance P (Fig. 2G′–H′ and Table S2B). The *I–V* curve showed that substance P-induced inward current in control neurons and reduced inward current in preBötC neurons lacking *Nalcn*, but not in the RTN lacking *Nalcn* (Fig. 2I and 2J), potentially explaining prior data from cultured hippocampal cells and slices containing the preBötC (Hayes and Del Negro, 2007; Lu et al., 2009).

Thus, although Nalcn is important for the resting membrane potential, firing frequency, and modulatory response to substance P, mice without Nalcn in RTN neurons are still able to sustain regular breathing. In the preBötC neurons, however, Nalcn current is critical for excitability, network stability, and modulatory response of substance P, as well as regular *in vivo* respiration.

Loss of *Nalcn* in the preBötC or Atoh1^{+} lineage leads to apneas during both sleep and wake periods

Given that we performed the UWBP during the daytime and found apneas while the animals were at rest (Fig. 1B and 1C), we hypothesized that the apneas also happened while the animals were asleep. Therefore, we performed UWBP from *Nalcn*$^{flox/flox}$, *Atoh1*^{Cre}; *Nalcn*$^{flox/+}$, *Nalcn*^{Atoh1CKO}, *Dbx1*^{Cre}; *Nalcn*$^{flox/+}$, and *Nalcn*^{Dbx1CKO} mice while recording electroencephalogram (EEG) and electromyogram (EMG) to categorize the apnea frequency in different states of brain activity (Fig. 3A–D). Compared to control mice, *Nalcn*^{Dbx1CKO} mice showed a much greater frequency of apnea during active wake, quiet wake, and both non-rapid eye movement (non-REM) and rapid eye movement (REM) stages of sleep (Fig. 3E and Fig. S4A). Similarly, *Nalcn*^{Atoh1CKO} mice had higher frequency of apnea in active wake, quiet wake, and non-REM stages (Fig. 3F and Fig. S4B). Moreover, *Nalcn*^{Dbx1CKO} mice showed longer apnea duration in quiescence or in sleep (Fig. S4C, left), unlike *Nalcn*^{Atoh1CKO} mice (Fig. S4C, right). The results indicate that Atoh1-dependent neurons and preBötC neurons require Nalcn to maintain regular breathing, likely because of reduction in the excitability of the respiratory center.

DISCUSSION

Nalcn is a nonselective cation channel that contributes to the majority of basal Na^{+} leak current and neuropeptide modulations (Ren, 2011). Mice lacking *Nalcn* show respiratory failure leading to death within 24 hours of birth, but the cellular mechanisms mediating this phenotype remained unknown. Here we have shown, first, that Nalcn in glutamatergic neurons is critical for survival, and we pinpointed the Dbx1^{+} glutamatergic preBötC neurons as a critical subpopulation for viability. Second, we have shown that Nalcn contributes to the establishment of resting membrane potential and thus neuronal excitability of the oscillatory populations within the RTN and the preBötC. Third, substance P modulates RTN and preBötC activity in a Nalcn-dependent manner. Fourth, Nalcn in either the preBötC or Atoh1^{+} lineage is essential for regular breathing, in both awake and sleep states.

Although *Nalcn* expressed by Dbx1^{+} glutamatergic neurons in the preBötC is essential for neonatal respiration, and loss of *Nalcn* alters the neuronal excitability of RTN and preBötC neurons, only a portion of the mice lacking *Nalcn* in the preBötC die (in contrast with *Nalcn*^{Vglut2CKO} mice). Compensatory mechanisms from other neurons within the respiratory network and tonic sources projecting to the central pattern generator could also sustain circuit performance, and thus form a robust network that is able to bypass the disturbance within the preBötC; it is also possible that decreased conductance from other unidentified outward potassium channels might partially suppress the *Nalcn* phenotype and equip survivors to have regular breathing and chemoresponses. Interestingly, adult *Nalcn*^{Atoh1CKO} mice but not *Nalcn*^{Phox2bCKO} mice show a greater tendency to have apnea. Among all the different Atoh1-dependent neurons within the pontine respiratory group, the parabrachial (PB) neurons express *Atoh1* but not *Phox2b* during development (Gray, 2008). It has been shown that the pontine respiratory group phase-selectively drives medullary post-inspiratory activity (Poon and Song, 2014). Future studies deleting *Nalcn* in PB neurons should reveal the role of Nalcn in these neurons in maintaining breathing.

Sleep apnea is increasingly appreciated to bring a risk of adverse cardiovascular events and mortality (Mansukhani et al., 2015). In this study, we reveal that the loss of *Nalcn* leads to increased apnea whereas loss of *Nalcn* in Dbx1^{+} preBötC neurons increased neonatal lethality. Loss of neurons within the preBötC have been shown to directly affect respiratory stability, especially during the transition to sleep (Gray et al., 2001; Hayes et al., 2012; McKay et al., 2005; Wang et al., 2014). Future discovery of specific pharmacological agonists for Nalcn would benefit the investigation of its physiological role and potential therapeutic strategies for respiratory disorders.

The TTX-resistant Nalcn current contributes to establishing the resting membrane potential of RTN and preBötC neurons, and stability of both networks, as well as the modulatory response to substance P. Compared to acute silencing of RTN neurons, which results in a reduced ventilatory response to hypercapnic challenge (Marina et al., 2010), RTN neurons lacking *Nalcn* are still able to sustain chemoreflexes in adulthood. A recent study showed that reducing *Nalcn* in the RTN by short-hairpin RNA (shRNA) does not alter the chemosensitivity of these neurons *ex vivo* but reduces their response to a hypercapnic environment *in vivo* (Shi et al., 2016). Here, using genetic cell-specific studies, we found both *Nalcn*^{Phox2bCKO} and *Nalcn*^{Atoh1CKO} mice showed a fairly normal response to hypercapnic challenge (Fig. S3A). The difference in our results could be due to the fact that genetic deletion, unlike the acute shRNA knockdown, might permit compensation during development. To bypass the developmental compensation, we generated adult knockout mice (aKO) using *Ubc*^{CreERT2} (Ruzankina et al., 2007) and reproduced several breathing phenotypes and premature lethality (Fig. S5), but did not observe the abnormal hypercapnic response. It is still feasible that the immediacy of an acute knockdown compromises the network more prominently than a gradual tamoxifen-induced knockout. Lastly, we used 5% CO_2; Shi *et al.* did not see an effect at 4% CO_2 but did see the abnormal hypercapnic response at 6 and 8% CO_2. The lack of chemosensory defects in adult mice suggests that ion channels besides Nalcn are responsible for detecting environmental changes. Indeed, a groundbreaking study has discovered that alkaline-activated TASK-2 channel and proton-activated receptor GPR4 are expressed within RTN neurons and both are essential central mediators of respiratory chemosensitivity *in vivo* (Guyenet et al., 2016; Kumar et al., 2015; Wang et al., 2013).

In addition to generating spontaneous rhythms, the respiratory network receives multiple inputs that induce the release of neuromodulators to regulate the frequency and amplitude of respiration (Doi and Ramirez, 2008). Substance P-evoked slow excitation and effects on respiratory frequency is conserved down to the lamprey (Bongianni et al., 2014), but the underlying channel in the respiratory network was unclear. Here we show that genetic removal of *Nalcn* from the Atoh1^{+} RTN and Dbx1^{+} preBötC neurons leads to a reduced response to substance P modulation. It is interesting to note that, unlike *Nalcn* mutant mice, *Tachykinin precursor 1* (*Tac1*)-null mice lacking substance P and neurokinin A show an attenuated hypoxic response (Berner et al., 2007), suggesting compensation from other neuromodulators (Doi and Ramirez, 2010).

In summary, through combining genetic, electrophysiological, and behavioral approaches, we have found that Nalcn current determines rhythmic activity and modulatory response to

substance P in both the RTN and preBötC. The biophysical properties of Nalcn current are distinct from the currents involved in the rhythmogenesis of preBötC, underscoring a specific role of Nalcn in the respiratory network. The *in vivo* results highlight the importance of Nalcn conductance in the stability of breathing and the potential usefulness of Nalcn agonists in the treatment of central apnea.

STAR★METHODS

KEY RESOURCES TABLE

REAGENT or RESOURCE	SOURCE	IDENTIFIER
Antibodies		
Chicken anti-GFP	Abcam	ab13970; RRID: AB_300798
Goat anti-Phox2b	Santa Cruz Biotechnology	sc-13226; RRID: AB_2163613
Chemicals, Peptides, and Recombinant Proteins		
Substance P	Tocris Bioscience	1156
Experimental Models: Organisms/Strains		
Mouse: *Nalcn*$^{flox/flox}$	This paper	
Mouse: C57BL/6J	The Jackson Laboratory	RRID: IMSR_JAX:000664
Mouse: *Hprt*^{Cre} (129S1/Sv-*Hprt*$^{tm1(CAG-cre)Mnn}$/J)	The Jackson Laboratory	RRID: IMSR_JAX:004302
Mouse: *Nestin*^{Cre} (B6.Cg-Tg(Nes-cre)1Kln/J)	The Jackson Laboratory	RRID: IMSR_JAX:003771
Mouse: *Vglut2*^{Cre} (*Slc17a6*$^{tm2(cre)Lowl}$/J)	The Jackson Laboratory	RRID: IMSR_JAX:016963
Mouse: *Viaat*^{Cre} (B6.FVB-Tg(Slc32a1-cre)2.1Hzo/FrkJ)	The Jackson Laboratory	RRID: IMSR_JAX:017535
Mouse: *Chat*^{Cre} (B6;129S6-*Chat*$^{tm2(cre)Lowl}$/J)	The Jackson Laboratory	RRID: IMSR_JAX:006410
Mouse: *Pet1*^{Cre} (B6.Cg-Tg(Fev-cre)1Esd/J)	The Jackson Laboratory	RRID: IMSR_JAX:012712
Mouse: *En1*^{Cre} (*En1*$^{tm2(cre)Wrst}$/J)	The Jackson Laboratory	RRID: IMSR_JAX:007916
Mouse: *Ubc*^{CreERT2} (B6.Cg-Tg(UBC-cre/ERT2)1Ejb/1J)	The Jackson Laboratory	RRID: IMSR_JAX:007001
Mouse: *Rosa*$^{LSL-tdTOMATO}$ (B6.Cg-*Gt(ROSA)26Sor*$^{tm14(CAG-tdTomato)Hze}$/J)	The Jackson Laboratory	RRID: IMSR_JAX:007914
Mouse: *Atoh1*^{Cre}	(Yang et al., 2010)	RRID: MGI:4844110
Mouse: *Phox2b*^{Cre}	(Scott et al., 2011)	RRID: IMSR_JAX:016223
Mouse: *Dbx1*^{Cre}	(Bielle et al., 2005)	RRID: IMSR_EM:01924
Software and Algorithms		
LabChart	ADInstruments	RRID: SCR_001620
Neuroscore	Data Sciences International	N/A
Matlab	Mathworks	RRID: SCR_001622
Ponemah 3	Data Sciences International	N/A
Python 3	Python Software Foundation	RRID: SCR_008394
Prism 6	GraphPad	N/A
ImageJ	National Institutes of Health	RRID: SCR_003070
Other		
i-STAT	Abbott	https://www.pointofcare.abbott/us/en/offerings/istat/istat-handheld
PhysioTel F20-EET telemetry transmitter	Data Sciences International	https://www.datasci.com/products/implantable-telemetry/mouse-(miniature)/f20-eet

CONTACT FOR REAGENT AND RESOURCE SHARING

Further information and requests for resources and reagents should be directed to, and will be fulfilled by the corresponding author, Dr. Huda Y. Zoghbi (hzoghbi@bcm.edu).

EXPERIMENTAL MODEL AND SUBJECT DETAILS

Mouse lines—Mice were housed in an AAALAS-certified Level 3 facility on a 14 hour light cycle. The following mouse models were used: *Nalcn*$^{flox/flox}$, *Hprt*^{Cre} (129S1/Sv-*Hprt*$^{tm1(CAG-cre)Mnn}$/J, JAX 004302), *Nestin*^{Cre} (B6.Cg-Tg(Nes-cre)1Kln/J, JAX 003771), *Vglut2*^{Cre} (*Slc17a6*$^{tm2(cre)Lowl}$/J, JAX 016963), *Viaat*^{Cre} (B6.FVB-Tg(Slc32a1-cre)2.1Hzo/FrkJ, JAX 017535), *Chat*^{Cre} (B6;129S6-*Chat*$^{tm2(cre)Lowl}$/J, JAX 006410), *Pet1*^{Cre} (B6.Cg-Tg(Fev-cre)1Esd/J, JAX 012712), *Atoh1*^{Cre}, *Phox2b*^{Cre}, *Dbx1*^{Cre}, *En1*^{Cre} (*En1*$^{tm2(cre)Wrst}$/J, JAX 007916), *Ubc*^{CreERT2} (B6.Cg-Tg(UBC-cre/ERT2)1Ejb/1J, JAX 007001), and *Rosa*$^{LSL-tdTOMATO}$ (B6.Cg-*Gt(ROSA)26Sor*$^{tm14(CAG-tdTomato)Hze}$/J, JAX 007914). For staging, noon on the day that the vaginal plug was observed counted as embryonic day 0.5 (E0.5). Tails were collected for PCR genotyping. For tamoxifen-induced adult knockout, 7-week-old mice were injected daily during 5 days intraperitoneal injections with tamoxifen (100 mg/kg) dissolved in corn oil (20 mg/ml), and one week after the injections (9-week-old), mRNA level was analyzed by qPCR. All husbandry and experimental procedures were reviewed and approved by the Institutional Animal Care and Use Committee (IACUC) of Baylor College of Medicine.

Generation of the *Nalcn* floxed mice—Germ-line transmitted mice were generated with an ES cell clone (in a C57BL/6/Taconic background) obtained from KOMP in which *Nalcn* exons 5 and 6 are floxed (Fig. S1A). The neomycin resistant gene was removed by crossing the mice with Flippase mice. The line was subsequently backcrossed to C57BL/6J (JAX 000664) for more than 10 generations. Mice homozygous for the floxed *Nalcn* allele have a normal life span without observable abnormalities, suggesting that the floxed allele does not interfere with the endogenous expression of *Nalcn*. Genomic PCR was used to identify the mutant. PCR genotyping of the *Nalcn*^{flox} allele used 5′ primer (TTGCTCATCACCTAAAGGCACTTGC) and 3′primer (CCACAGTCCCCATTTGGCCATACTCTGAAA) primers (WT, 0.4 Kb; *Nalcn*^{flox}, 0.5 Kb; Fig. S1D).

METHOD DETAILS

Fluorescent activated cell sorting (FACS)—The RTN and cRL populations were identified by their anatomical position and morphology. The hindbrain of eight E16.5 *Atoh1*$^{EGFP/EGFP}$ embryos were dissected in cold Dulbecco's Modified Eagle's Medium (DMEM, serum free) and collected into 5 ml of Hank's Balanced Salt Solution (HBSS) in a 50 ml tube. After addition of 1 ml of 0.25% trypsin (Invitrogen) and 50 μl of DNase I (0.1%; ROCHE), the tube was incubated at 37 °C for 20 min. The reaction was stopped with 1 ml of high BSA buffer (HBSS with 8 mg/ml of BSA), and gently dissociated with a 10 ml syringe attached to the 18G and 22 ½G needles. Debris was filtered out using a 100 μm cell strainer (Falcon), and the combined cells from pooled embryos were collected using a table-top centrifuge (10 minutes, 1,000 x g, room temperature). The cell pellet was re-suspended in 1 ml of low BSA buffer (HBSS with 2 mg/ml BSA and 0.1% EDTA), and FACS was performed according to the respective brightness of enhanced green fluorescent protein (EGFP). For each sorting, EGFP negative and positive cells were collected directly into TRIzol LS reagent (Invitrogen), and stored at the −80°C freezer until RNA extraction. FACSAria I and II cytometers (BD Biosciences) were used for sorting and cell analysis.

RNA isolation and quantitative RT-PCR (qRT-PCR)—Total RNA from FACS purified cells was prepared by TRIzol method following manufacturer's instruction (Invitrogen). Pre-amplification and reverse transcription was performed using the Phi 29 polymerase-based QuantiTect whole transcriptome Kit (Qiagen). 10 ng of cDNA was used in triplicate for qPCR using SYBR Green FastMix (Quanta Biosciences).

***In situ* staining—**Frozen mouse sections (20 μm thick) were used for in situ staining. DNA templates were amplified from reverse-transcribed cDNA from P0 C57/B6 brainstem according to Allen Brain Atlas (www.brain-map.org) for *tdTOMATO, Unc79,* and *Unc80* DNA. *Nalcn* DNA fragment of 1811 bp, starting from nucleotide 4764, were amplified from the cDNA mentioned above. DNA fragments were subcloned into pGEM-T for single-strand, digoxigenin (DIG) or fluorescein-labeled RNA probe synthesis. Hybridization signals were visualized anti-DIG antibody, anti-fluorescein, and tyramide signal amplification kits (Thermo Fisher Scientific), and detected by a Leica TCS SP8 confocal system. Image brightness and contrast were normalized using image J.

Immunofluorescence (IF) assay—IF and cryosectioning were performed as previously described (Huang et al., 2012). Briefly, frozen sections were cut with 20 μm thickness. The primary antibodies and antiserum used are: chicken anti-GFP (1:1000, Abcam) and goat anti-Phox2b (1:500, Santa Cruz). Secondary antibodies were conjugated with Alexa Fluor 488 or 555 (1:2000, Molecular Probes). We used a Leica TCS SP5 confocal system to detect fluorescent staining. Image brightness and contrast were normalized using Image J and Adobe Photoshop.

Neonatal head-out pneumotachography—P0 respiration from transgenic mice and littermate controls was measured in a custom built head-out mask and pneumotachograph system that was engineered and machined for a minimum of dead space to increase sensitivity. Additional facemask ports were engineered for gas flow-through and calibration. For calibration and experiments, room air was drawn through the mask-pneumotachograph and O_2 and CO_2 analyzers (AEI) by a vacuum pump attached to the gas flow-through port. All measurements were done between 7 am and 1 pm on the day of birth. Prior to an experiment, the facemask was sealed with a piece of nitrile rubber. Ventilation was calibrated as a series of 20 μl pipetman injections into an empty facemask at a rate of 3 Hz. The rate of gas flow-through (12.5 mL/min) was continuously controlled via a rotameter. For experimental assays, a small opening was made in the nitrile rubber to fit the snout (nose and mouth) of a P0.5 mouse. The mouse was affixed to the facemask with Impregum F, Polyether Impression material (Patterson Dental, St. Paul, MN, USA). The mouse rested on a platform attached to the facemask that fit inside a temperature controlled chamber to maintain the mouse pup at 36°C. Pneumotachograph pressure changes were measured by a Validyne DP45 differential pressure transducer and CD15 carrier demodulator and recorded with LabChartPro (AD Instruments, Colorado Springs, CO, USA) in real time. The pneumotachograph trace was integrated to produce a respiratory waveform. Waveforms were analyzed offline to determine respiratory rate (V_f), tidal volume (V_T), minute ventilation (V_E) and pattern analysis. Tidal volume (V_T) was determined by comparing peak (mV) height to calibration injections (mV/μl). O_2 consumption was determined by comparing the

gas composition between calibration in the empty chamber without the mouse pup and live breathing using an AEI oxygen sensor and analyzer. Chamber temperature was constantly monitored using a ThermoWorks MicroThermo 2 and probe and was recorded with LabChartPro in real time. After attachment to the facemask, mice were allowed to acclimate for 10 min in room air followed by 20 minutes of data collection. Respiratory waveforms were collected when the neonate was at rest and readings were free from movement artifacts. A minimum of 1 minute of cumulative data compiled from traces at least 10 seconds long from the last 10 minutes of the assay were analyzed. Apart from integration, no filtering, smoothing or other manipulations were applied to the pressure waveform. Apneas were defined as an inter-breath interval that was longer than 3 seconds. Values given are means and standard deviation (SD).

Unrestrained whole-body plethysmography (UWBP)—Breathing analysis has been described previously (Huang et al., 2012) with some modifications. Adult mice were placed within the unrestrained whole-body plethysmography (UWBP) chambers (Buxco), with a continuous flow rate of 0.5 liter/min flushing the chambers with fresh air. Breath waveforms and derived parameters, including the instantaneous breathing rate, tidal volume, inspiratory time, expiratory time, and apnea frequency, were captured using Ponemah 3 software (DSI) and processed using Matlab (Mathworks). Mice were allowed to acclimate for at least 20 min, and baseline breathing was recorded for at least 20 min (baseline). No significant differences were found between any respiratory parameters of the male and female mice, hence they were grouped together. To determine response to hypercapnic gas, the chamber was flushed with hypercapnic gas (5% CO_2, 20% O_2 balanced with N_2 or 5% CO_2 balanced with O_2) for 15 min and breathing was recorded for the first 5 min of hypercapnic exposure (hypercapnia), and allowed to recover in fresh air for 15 min (recovery). Hypoxic gas (10% O_2 balanced with N_2) challenge was done in the same manner. To reduce artifacts from excessive movement and sniffing behavior, breaths that exhibited an inspiratory time less than 0.025 seconds, an expiratory time greater than 10 seconds, and a calculated exhaled tidal volume over 200% or under 50% of calculated inhaled tidal volume were excluded; additionally, a sliding window of 200 breaths was used to filter out intervals where more than 10% of breaths in the window were above 500 breaths per minute. Apneas were defined as breath periods at least 0.5 seconds in duration, at least twice the duration of the 6 surrounding breaths, and at least twice the duration of the average breath during the baseline recording. Values given are means and standard deviation (SD). Statistical significance was tested using ANOVA; significance was accepted at p-values lower than 0.05. To analyze the regularity of breathing, the calculation has been described previously (Holt et al., 1996). In brief, covariance (CV) is calculated as the ratio between the standard deviation of breath length and the mean breath length of any given animal, and CV2 measures the variability in breath lengths between two following breaths: CV2=2*abs [breath length(n)-breath length(n-1)]/[breath length(n)+breath length(n-1).

Sleep apnea recording

Implantation of transmitters and electrode leads: Adult mice at 12–15 weeks (body weight 20–30 g) were anesthetized with isoflurane and mounted in a stereotaxic frame. Under aseptic condition, a 2.5–3.0 cm incision was made through the skin along the dorsal

midline from the posterior margin of the eyes to a midway between the scapulae. Then, a subcutaneous pocket was formed using small, blunt-tipped dissecting scissors from the neck incision across the back and down along the animal's flank. Once the pocket is formed, irrigate the tunnel with sterile saline and insert the transmitter (F20-EET, DSI) through the incision on the dorsal head/neck region into the subcutaneous pocket with the flatter side of the device against the muscle and the biopotential leads oriented cranially. The transmitter was positioned along the dorsal flank between the forelimb and hind limb. The bare U-shaped end parts of the electrode leads of Channel 1 were implanted into the subdural space of the left frontal (A1.0L1.0, negative) and right parietal (P3.0R3.0, positive) cortex for the recordings of electroencephalogram (EEG) (Paxinos et al., 2001). The leads of Channel 2 were bared for about 2.0 mm at ends and implanted into the neck muscles for the monitoring of electromyogram (EMG). All of the electrode leads were fixed in place with dental cement on the skull. Animals were allowed 7–10 days to recover before data collection.

Telemetry and plethysmography: EEG, EMG, and activity outputs were recorded by using a receiver matrix coupled to Ponemah 3 software (DSI). EEG and EMG data were divided into 10-second epochs, where a sleep stage was semi-automatically assigned using the Sleep module of Neuroscore (DSI). When activity is above the threshold (i.e., 10), it overrides all other parameters and the epoch is assigned as active wake. EMG and EEG were used to assign active wake, quiet wake, non-REM sleep, or REM sleep. EMG has a high tone during active wake and a threshold of 0.05 mV was used. Delta power (0.5–4 Hz) is the dominant factor in non-REM sleep. A threshold of 0.6 was used for the delta ratio, which is the ratio of delta power over total power (0.5–25 Hz). Theta power (6–9 Hz) is dominant during REM sleep. A threshold of 3 was used for the theta ratio, which is the ratio of theta power over delta power. Once the epochs were assigned a stage by the algorithm, visual inspection was performed to verify and correct the scoring if necessary.

Breath waveforms and derived parameters were captured using Ponemah 3 software (DSI) and processed using Python 3 (Python Software Foundation). Apneas were defined as breath periods at least 0.5 seconds in duration, at least twice the duration of the 6 surrounding breaths, and at least twice the duration of the average breath during the baseline recording. Values given are means and standard deviation (SD). Statistical significance was tested using ANOVA; significance was accepted at p-values lower than 0.05.

Physiological analyses

RTN medullary slice preparation: For RTN recording in slice, details regarding the preparation of brain slices have been described previously (Mulkey et al., 2007) with some modifications. All data acquisition and analyses were carried out blinded to genotype. P0 *Atoh1*^{Cre}*; Nalcn*$^{flox/+}$*; Rosa*^{tdTOMATO} and *Nalcn*^{Atoh1CKO}*; Rosa*^{tdTOMATO} mice were decapitated under hypothermia anesthesia and transverse slices (500 μm thick) were prepared from the medullary brainstem in the region of the RTN with a vibratome (VT1200, Leica Microsystems) in a chamber filled with chilled (2–5°C) cutting solution containing (in mM) 120 sucrose, 59.5 NaCl, 2.75 KCl, 1.25 $CaCl_2$, 3.5 $MgCl_2$, 0.5 $MgSO_4$, 1.25 $NaH2PO_4$, 25.6 $NaHCO_3$, 9 D-glucose. The medullary slices were then incubated in artificial cerebrospinal fluid (aCSF, in mM) containing 119 NaCl, 26.2 $NaHCO_3$, 11 D-

glucose, 3 KCl, 2 $CaCl_2$, 1 $MgSO_4$, 1.25 NaH_2PO_4 at 37°C for 30 min and subsequently at the room temperature equilibrated with 95% O_2/5% CO_2.

PreBötC medullary slice preparation: For preBötC recording in slice, details regarding the preparation of brain slices have been described previously (Picardo et al., 2013). All data acquisition and analyses were carried out blinded to genotype. P0 *Dbx1*^{Cre}*; Nalcn*$^{flox/+}$*; Rosa*^{tdTOMATO} and *Nalcn*^{Dbx1CKO}*; Rosa*^{tdTOMATO} mice were decapitated under hypothermia anesthesia and transverse slices (650 μm thick), which were endogenously rhythmically active slices producing a respiratory-related rhythm, were prepared from the medullary brainstem in the region of the preBötC with a vibratome (Leica Microsystems) in a chamber filled with chilled (2–5°C) artificial cerebrospinal fluid (aCSF, in mM) containing 124 NaCl, 25 $NaHCO_3$, 30 D-glucose, 3 KCl, 1.5 $CaCl_2$, 1 $MgSO_4$, and 0.5 NaH_2PO_4. The slices were then incubated in aCSF at the room temperature and equilibrated with 95% O_2 and 5% CO_2. Potassium concentration was increased to 9 mM to stimulate the spontaneous rhythmic respiratory motor discharge in the medullary slice.

Recording and analysis: Whole-cell recording was made using patch-clamp amplifiers (MultiClamp 700B, Molecular Devices, Union City, CA) under infrared–differential interference contrast microscopy (Zeiss). Data acquisition and analysis were performed using digitizers (DigiData 1440A, Molecular Devices) and analysis software pClamp 10 (Molecular Devices) and 6.0.7 (Synaptosoft Inc.). Signals were filtered at 2 kHz and sampled at 10 kHz. The intra-pipette solution for current-clamp recordings contained (in mM) 140 potassium gluconate, 5 KCl, 10 HEPES, 0.2 EGTA, 2 $MgCl_2$, 4 MgATP, 0.3 Na_2GTP and 10 Na_2-phosphocreatine, pH 7.2 (with KOH). Voltage-clamp experiments used aCSF containing 1 μM TTX and intrapipette solution contained (in mM) 140 $CsMeSO_4$, 5 TEA-Cl, 10 HEPES, 1 EGTA, 2 $MgCl_2$, 2.5 MgATP, 0.3 Na_2GTP, pH 7.2. Substance P (1 μM) was dissolved in aCSF. In brief, borosilicate glass microelectrodes (King Precision Glass, Inc.) were pulled by a micropipette puller (Model P-1000, Sutter Instrument, USA) was placed on the surface of the brain slice in an area of the ventral respiratory group, containing the preBötC neurons, with Microelectrode AC Amplifier Model 1800 (A-M Systems). The preBötC was identified based on its proximity to anatomical landmarks, such as the nucleus ambiguus and the inferior olive. LabChart 8 (ADInstruments) was used to analyze population recordings of burst frequency and amplitude. Values given are means and standard deviation (SD). Statistical significance was tested using either Student's t test or ANOVA; significance was accepted at p-values lower than 0.05.

Blood gas measurements—Arterial blood sample was collected by thoracotomy using 1 ml syringe and 25 gauge needle while the animal was anesthetized with isoflurane and mounted in a stereotaxic frame. Blood sample analysis was performed by iSTAT® system using CG8+ cartridge (Abbott). Values given are means and standard deviation (SD).

QUANTIFICATION AND STATISTICAL ANALYSIS

Statistics—Prism 6 software (GraphPad) was used to analyze the data. All comparisons were two sided. Student's t-test or ANOVA were used throughout; chi-square test was used

in Table 1; log-rank test was used in Figure S5. All the data are expressed as mean ± standard deviation (SD).

Supplementary Material

Refer to Web version on PubMed Central for supplementary material.

Acknowledgments

We thank members of the Zoghbi laboratory for helpful discussions and V. Brandt for comments on the manuscript. We thank Drs. J. Elmquist, L. Gan, A. Pierani, and A. Joyner for the *Phox2b*^{Cre}, *Atoh1*^{Cre}, *Dbx1*^{Cre}, and *En1*^{Cre} mice, respectively. This work was supported by an American Heart Association SouthWest affiliate Predoctoral Fellowship to W.-H.H. (11PRE6080004), National Institute of Neurological Disorders and Stroke to D.R. (NS055293 and NS074257) and M.X. (R01NS100893), Citizens United for Research in Epilepsy to M.X., the RNA In Situ and Microscopy, the Neurobehavior, and the Neuroconnectivity Cores of the Baylor College of Medicine Intellectual and Developmental Disabilities Research Center (HD083092 and U54HD083092), the *In Vivo* Neurophysiology Core at Texas Children's Hospital, the Cytometry and Cell Sorting Core at Baylor College of Medicine with funding from the NIH (P30 AI036211, P30 CA125123, and S10 RR024574) and the expert assistance of Joel M. Sederstrom, and Howard Hughes Medical Institute to H.Y.Z. M.X. is a Caroline DeLuca Scholar.

References

Berner J, Shvarev Y, Lagercrantz H, Bilkei-Gorzo A, Hokfelt T, Wickstrom R. Altered respiratory pattern and hypoxic response in transgenic newborn mice lacking the tachykinin-1 gene. J Appl Physiol. 2007; 103:552–559. [PubMed: 17525292]

Bielle F, Griveau A, Narboux-Neme N, Vigneau S, Sigrist M, Arber S, Wassef M, Pierani A. Multiple origins of Cajal-Retzius cells at the borders of the developing pallium. Nat Neurosci. 2005; 8:1002–1012. [PubMed: 16041369]

Bongianni F, Mutolo D, Cinelli E, Pantaleo T. Neural mechanisms underlying respiratory rhythm generation in the lamprey. Respir Physiol Neurobiol. 2016; 224:17–26. [PubMed: 25220696]

Bouvier J, Thoby-Brisson M, Renier N, Dubreuil V, Ericson J, Champagnat J, Pierani A, Chedotal A, Fortin G. Hindbrain interneurons and axon guidance signaling critical for breathing. Nat Neurosci. 2010; 13:1066–1074. [PubMed: 20680010]

Chao HT, Chen H, Samaco RC, Xue M, Chahrour M, Yoo J, Neul JL, Gong S, Lu HC, Heintz N, et al. Dysfunction in GABA signalling mediates autism-like stereotypies and Rett syndrome phenotypes. Nature. 2010; 468:263–269. [PubMed: 21068835]

Chong JX, McMillin MJ, Shively KM, Beck AE, Marvin CT, Armenteros JR, Buckingham KJ, Nkinsi NT, Boyle EA, Berry MN, et al. De novo mutations in NALCN cause a syndrome characterized by congenital contractures of the limbs and face, hypotonia, and developmental delay. Am J Hum Genet. 2015; 96:462–473. [PubMed: 25683120]

Del Negro CA, Morgado-Valle C, Feldman JL. Respiratory rhythm: an emergent network property? Neuron. 2002; 34:821–830. [PubMed: 12062027]

Doi A, Ramirez JM. Neuromodulation and the orchestration of the respiratory rhythm. Respir Physiol Neurobiol. 2008; 164:96–104. [PubMed: 18602029]

Doi A, Ramirez JM. State-dependent interactions between excitatory neuromodulators in the neuronal control of breathing. J Neurosci. 2010; 30:8251–8262. [PubMed: 20554877]

Dubreuil V, Thoby-Brisson M, Rallu M, Persson K, Pattyn A, Birchmeier C, Brunet JF, Fortin G, Goridis C. Defective respiratory rhythmogenesis and loss of central chemosensitivity in Phox2b mutants targeting retrotrapezoid nucleus neurons. J Neurosci. 2009; 29:14836–14846. [PubMed: 19940179]

Feldman JL, Del Negro CA, Gray PA. Understanding the rhythm of breathing: so near, yet so far. Annu Rev Physiol. 2013; 75:423–452. [PubMed: 23121137]

Gal M, Magen D, Zahran Y, Eran A, Khayat M, Gafni C, Levanon EY, Mandel H. A novel homozygous splice site mutation in NALCN identified in siblings with Cachexia, Strabismus,

Severe Intellectual Disability, Epilepsy and Abnormal Respiratory Rhythm. Eur J Med Genet. 2016; 59:204–209. [PubMed: 26923739]

Gray PA. Transcription factors and the genetic organization of brain stem respiratory neurons. J Appl Physiol. 2008; 104:1513–1521. [PubMed: 18218908]

Gray PA, Hayes JA, Ling GY, Llona I, Tupal S, Picardo MC, Ross SE, Hirata T, Corbin JG, Eugenin J, et al. Developmental origin of preBotzinger complex respiratory neurons. J Neurosci. 2010; 30:14883–14895. [PubMed: 21048147]

Gray PA, Janczewski WA, Mellen N, McCrimmon DR, Feldman JL. Normal breathing requires preBotzinger complex neurokinin-1 receptor-expressing neurons. Nat Neurosci. 2001; 4:927–930. [PubMed: 11528424]

Guyenet PG, Bayliss DA, Stornetta RL, Ludwig MG, Kumar NN, Shi Y, Burke PG, Kanbar R, Basting TM, Holloway BB, et al. Proton detection and breathing regulation by the retrotrapezoid nucleus. J Physiol. 2016; 594:1529–1551. [PubMed: 26748771]

Hayes JA, Del Negro CA. Neurokinin receptor-expressing pre-botzinger complex neurons in neonatal mice studied in vitro. J Neurophysiol. 2007; 97:4215–4224. [PubMed: 17409172]

Hayes JA, Wang X, Del Negro CA. Cumulative lesioning of respiratory interneurons disrupts and precludes motor rhythms in vitro. Proc Natl Acad Sci USA. 2012; 109:8286–8291. [PubMed: 22566628]

Hodges MR, Wehner M, Aungst J, Smith JC, Richerson GB. Transgenic mice lacking serotonin neurons have severe apnea and high mortality during development. J Neurosci. 2009; 29:10341–10349. [PubMed: 19692608]

Holt GR, Softky WR, Koch C, Douglas RJ. Comparison of discharge variability in vitro and in vivo in cat visual cortex neurons. J Neurophysiol. 1996; 75:1806–1814. [PubMed: 8734581]

Huang WH, Tupal S, Huang TW, Ward CS, Neul JL, Klisch TJ, Gray PA, Zoghbi HY. Atoh1 governs the migration of postmitotic neurons that shape respiratory effectiveness at birth and chemoresponsiveness in adulthood. Neuron. 2012; 75:799–809. [PubMed: 22958821]

Ishihara N, Armsen W, Papadopoulos T, Betz H, Eulenburg V. Generation of a mouse line expressing Cre recombinase in glycinergic interneurons. Genesis. 2010; 48:437–445. [PubMed: 20506101]

Jacquin TD, Borday V, Schneider-Maunoury S, Topilko P, Ghilini G, Kato F, Charnay P, Champagnat J. Reorganization of pontine rhythmogenic neuronal networks in Krox-20 knockout mice. Neuron. 1996; 17:747–758. [PubMed: 8893031]

Janczewski WA, Tashima A, Hsu P, Cui Y, Feldman JL. Role of inhibition in respiratory pattern generation. J Neurosci. 2013; 33:5454–5465. [PubMed: 23536061]

Kimmel RA, Turnbull DH, Blanquet V, Wurst W, Loomis CA, Joyner AL. Two lineage boundaries coordinate vertebrate apical ectodermal ridge formation. Genes Dev. 2000; 14:1377–1389. [PubMed: 10837030]

Koizumi H, Smerin SE, Yamanishi T, Moorjani BR, Zhang R, Smith JC. TASK channels contribute to the K+-dominated leak current regulating respiratory rhythm generation in vitro. J Neurosci. 2010; 30:4273–4284. [PubMed: 20335463]

Kumar NN, Velic A, Soliz J, Shi Y, Li K, Wang S, Weaver JL, Sen J, Abbott SB, Lazarenko RM, et al. PHYSIOLOGY Regulation of breathing by CO(2) requires the proton-activated receptor GPR4 in retrotrapezoid nucleus neurons. Science. 2015; 348:1255–1260. [PubMed: 26068853]

Lu B, Su Y, Das S, Liu J, Xia J, Ren D. The neuronal channel NALCN contributes resting sodium permeability and is required for normal respiratory rhythm. Cell. 2007; 129:371–383. [PubMed: 17448995]

Lu B, Su Y, Das S, Wang H, Wang Y, Liu J, Ren D. Peptide neurotransmitters activate a cation channel complex of NALCN and UNC-80. Nature. 2009; 457:741–744. [PubMed: 19092807]

Lu B, Zhang Q, Wang H, Wang Y, Nakayama M, Ren D. Extracellular calcium controls background current and neuronal excitability via an UNC79-UNC80-NALCN cation channel complex. Neuron. 2010; 68:488–499. [PubMed: 21040849]

Madisen L, Zwingman TA, Sunkin SM, Oh SW, Zariwala HA, Gu H, Ng LL, Palmiter RD, Hawrylycz MJ, Jones AR, et al. A robust and high-throughput Cre reporting and characterization system for the whole mouse brain. Nat Neurosci. 2010; 13:133–140. [PubMed: 20023653]

Mansukhani MP, Wang S, Somers VK. Sleep, death, and the heart. American journal of physiology Heart and circulatory physiology. 2015; 309:H739–749. [PubMed: 26188022]

Marina N, Abdala AP, Trapp S, Li A, Nattie EE, Hewinson J, Smith JC, Paton JF, Gourine AV. Essential role of Phox2b-expressing ventrolateral brainstem neurons in the chemosensory control of inspiration and expiration. J Neurosci. 2010; 30:12466–12473. [PubMed: 20844141]

McKay LC, Janczewski WA, Feldman JL. Sleep-disordered breathing after targeted ablation of preBotzinger complex neurons. Nat Neurosci. 2005; 8:1142–1144. [PubMed: 16116455]

Mulkey DK, Rosin DL, West G, Takakura AC, Moreira TS, Bayliss DA, Guyenet PG. Serotonergic neurons activate chemosensitive retrotrapezoid nucleus neurons by a pH-independent mechanism. J Neurosci. 2007; 27:14128–14138. [PubMed: 18094252]

Pagliardini S, Janczewski WA, Tan W, Dickson CT, Deisseroth K, Feldman JL. Active expiration induced by excitation of ventral medulla in adult anesthetized rats. J Neurosci. 2011; 31:2895–2905. [PubMed: 21414911]

Paxinos, G., Franklin, KBJ., Franklin, KBJ. The mouse brain in stereotaxic coordinates. 2. San Diego: Academic Press; 2001.

Pena F, Ramirez JM. Substance P-mediated modulation of pacemaker properties in the mammalian respiratory network. J Neurosci. 2004; 24:7549–7556. [PubMed: 15329402]

Picardo MC, Weragalaarachchi KT, Akins VT, Del Negro CA. Physiological and morphological properties of Dbx1-derived respiratory neurons in the pre-Botzinger complex of neonatal mice. J Physiol. 2013; 591:2687–2703. [PubMed: 23459755]

Poon CS, Song G. Bidirectional plasticity of pontine pneumotaxic postinspiratory drive: implication for a pontomedullary respiratory central pattern generator. Prog Brain Res. 2014; 209:235–254. [PubMed: 24746051]

Ptak K, Yamanishi T, Aungst J, Milescu LS, Zhang R, Richerson GB, Smith JC. Raphe neurons stimulate respiratory circuit activity by multiple mechanisms via endogenously released serotonin and substance P. J Neurosci. 2009; 29:3720–3737. [PubMed: 19321769]

Ramirez JM, Dashevskiy T, Marlin IA, Baertsch N. Microcircuits in respiratory rhythm generation: commonalities with other rhythm generating networks and evolutionary perspectives. Curr Opin Neurobiol. 2016; 41:53–61. [PubMed: 27589601]

Ren D. Sodium leak channels in neuronal excitability and rhythmic behaviors. Neuron. 2011; 72:899–911. [PubMed: 22196327]

Revill AL, Vann NC, Akins VT, Kottick A, Gray PA, Del Negro CA, Funk GD. Dbx1 precursor cells are a source of inspiratory XII premotoneurons. eLife. 2015; 4

Rose MF, Ren J, Ahmad KA, Chao HT, Klisch TJ, Flora A, Greer JJ, Zoghbi HY. Math1 is essential for the development of hindbrain neurons critical for perinatal breathing. Neuron. 2009; 64:341–354. [PubMed: 19914183]

Rossi J, Balthasar N, Olson D, Scott M, Berglund E, Lee CE, Choi MJ, Lauzon D, Lowell BB, Elmquist JK. Melanocortin-4 receptors expressed by cholinergic neurons regulate energy balance and glucose homeostasis. Cell Metab. 2011; 13:195–204. [PubMed: 21284986]

Ruffault PL, D'Autreaux F, Hayes JA, Nomaksteinsky M, Autran S, Fujiyama T, Hoshino M, Hagglund M, Kiehn O, Brunet JF, et al. The retrotrapezoid nucleus neurons expressing Atoh1 and Phox2b are essential for the respiratory response to CO(2). eLife. 2015; 4

Ruzankina Y, Pinzon-Guzman C, Asare A, Ong T, Pontano L, Cotsarelis G, Zediak VP, Velez M, Bhandoola A, Brown EJ. Deletion of the developmentally essential gene ATR in adult mice leads to age-related phenotypes and stem cell loss. Cell Stem Cell. 2007; 1:113–126. [PubMed: 18371340]

Scott MM, Williams KW, Rossi J, Lee CE, Elmquist JK. Leptin receptor expression in hindbrain Glp-1 neurons regulates food intake and energy balance in mice. J Clin Invest. 2011; 121:2413–2421. [PubMed: 21606595]

Scott MM, Wylie CJ, Lerch JK, Murphy R, Lobur K, Herlitze S, Jiang W, Conlon RA, Strowbridge BW, Deneris ES. A genetic approach to access serotonin neurons for in vivo and in vitro studies. Proc Natl Acad Sci USA. 2005; 102:16472–16477. [PubMed: 16251278]

Shi Y, Abe C, Holloway BB, Shu S, Kumar NN, Weaver JL, Sen J, Perez-Reyes E, Stornetta RL, Guyenet PG, et al. Nalcn Is a “Leak” Sodium Channel That Regulates Excitability of Brainstem Chemosensory Neurons and Breathing. J Neurosci. 2016; 36:8174–8187. [PubMed: 27488637]

Smith JC, Ellenberger HH, Ballanyi K, Richter DW, Feldman JL. Pre-Botzinger complex: a brainstem region that may generate respiratory rhythm in mammals. Science. 1991; 254:726–729. [PubMed: 1683005]

Smith JC, Morrison DE, Ellenberger HH, Otto MR, Feldman JL. Brainstem projections to the major respiratory neuron populations in the medulla of the cat. J Comp Neurol. 1989; 281:69–96. [PubMed: 2466879]

Thoby-Brisson M, Karlen M, Wu N, Charnay P, Champagnat J, Fortin G. Genetic identification of an embryonic parafacial oscillator coupling to the preBotzinger complex. Nat Neurosci. 2009; 12:1028–1035. [PubMed: 19578380]

Thoby-Brisson M, Telgkamp P, Ramirez JM. The role of the hyperpolarization-activated current in modulating rhythmic activity in the isolated respiratory network of mice. J Neurosci. 2000; 20:2994–3005. [PubMed: 10751452]

Tronche F, Kellendonk C, Kretz O, Gass P, Anlag K, Orban PC, Bock R, Klein R, Schutz G. Disruption of the glucocorticoid receptor gene in the nervous system results in reduced anxiety. Nat Genet. 1999; 23:99–103. [PubMed: 10471508]

Vong L, Ye C, Yang Z, Choi B, Chua S Jr, Lowell BB. Leptin action on GABAergic neurons prevents obesity and reduces inhibitory tone to POMC neurons. Neuron. 2011; 71:142–154. [PubMed: 21745644]

Wang S, Benamer N, Zanella S, Kumar NN, Shi Y, Bevengut M, Penton D, Guyenet PG, Lesage F, Gestreau C, et al. TASK-2 channels contribute to pH sensitivity of retrotrapezoid nucleus chemoreceptor neurons. J Neurosci. 2013; 33:16033–16044. [PubMed: 24107938]

Wang X, Hayes JA, Revill AL, Song H, Kottick A, Vann NC, LaMar MD, Picardo MC, Akins VT, Funk GD, et al. Laser ablation of Dbx1 neurons in the pre-Botzinger complex stops inspiratory rhythm and impairs output in neonatal mice. eLife. 2014; 3:e03427. [PubMed: 25027440]

Yang H, Xie X, Deng M, Chen X, Gan L. Generation and characterization of Atoh1-Cre knock-in mouse line. Genesis. 2010; 48:407–413. [PubMed: 20533400]

Highlights

- Robust neonatal survival requires Nalcn in the preBötC.
- Nalcn contributes to the biophysical properties of the preBötC and the RTN.
- Substance P modulates preBötC and RTN network activity in a Nalcn-dependent manner.
- Loss of Nalcn in either the preBötC or Atoh1^{+} lineage leads to central apnea.

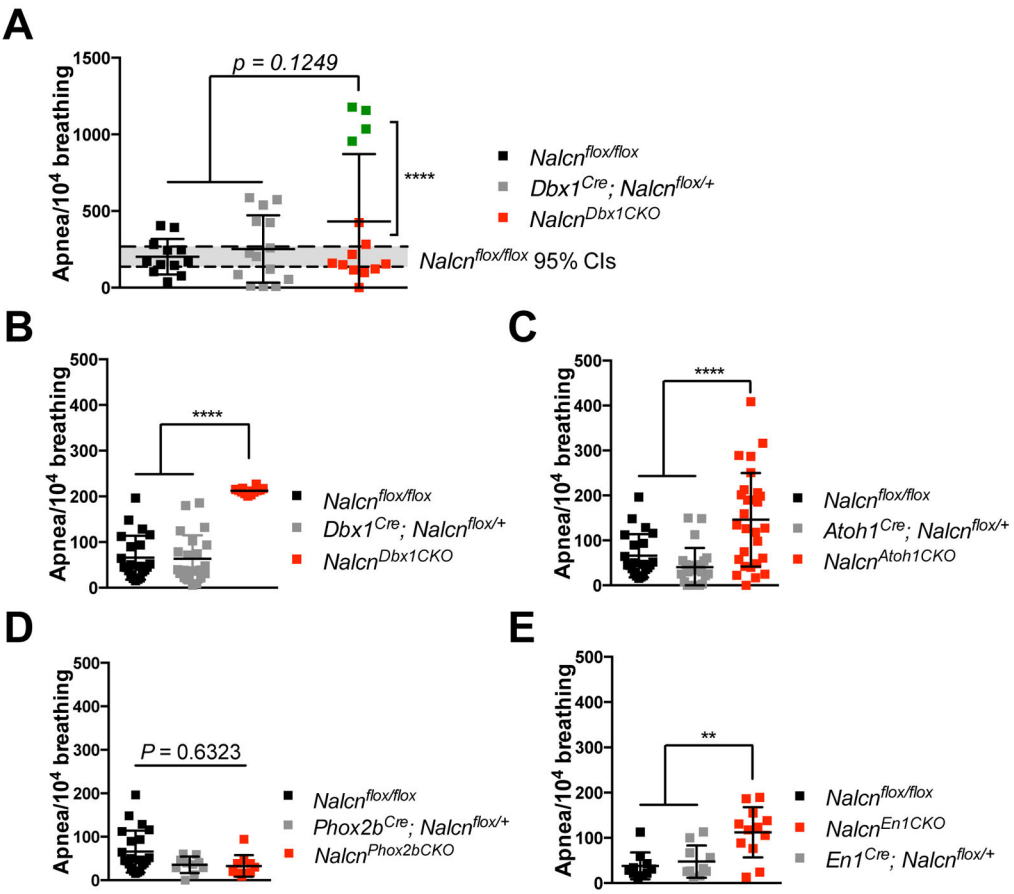

Figure 1. Loss of *Nalcn* in the preBötC and Atoh1$^+$ lineage leads to increased apneas

(A) Respiration recording from P0 *Nalcn$^{flox/flox}$* (n=12); *Dbx1^{Cre}; Nalcn$^{flox/+}$* (n=14); and *Nalcn^{Dbx1CKO}* (n=14) mice.

(B) Unrestrained whole-body plethysmography (UWBP) of 7-week-old *Nalcn$^{flox/flox}$* (n=22); *Dbx1^{Cre}; Nalcn$^{flox/+}$* (n=23); and *Nalcn^{Dbx1CKO}* (n=12) mice.

(C) UWBP of 7-week-old *Nalcn$^{flox/flox}$* (n=22), *Atoh1^{Cre}; Nalcn$^{flox/+}$* (n=24), and *Nalcn^{Atoh1CKO}* (n=28).

(D) UWBP of 7-week-old *Nalcn$^{flox/flox}$* (n=22), *Phox2b^{Cre}; Nalcn$^{flox/+}$* (n=10), and *Nalcn^{Phox2bCKO}* (n=10).

(E) UWBP of 7-week-old *Nalcn$^{flox/flox}$* (n=10), *En1^{Cre}; Nalcn$^{flox/+}$* (n=10), and *Nalcn^{En1CKO}* (n=12).

One-way ANOVA, mean ± SD, **: $P < 0.01$; ****: $P < 0.001$

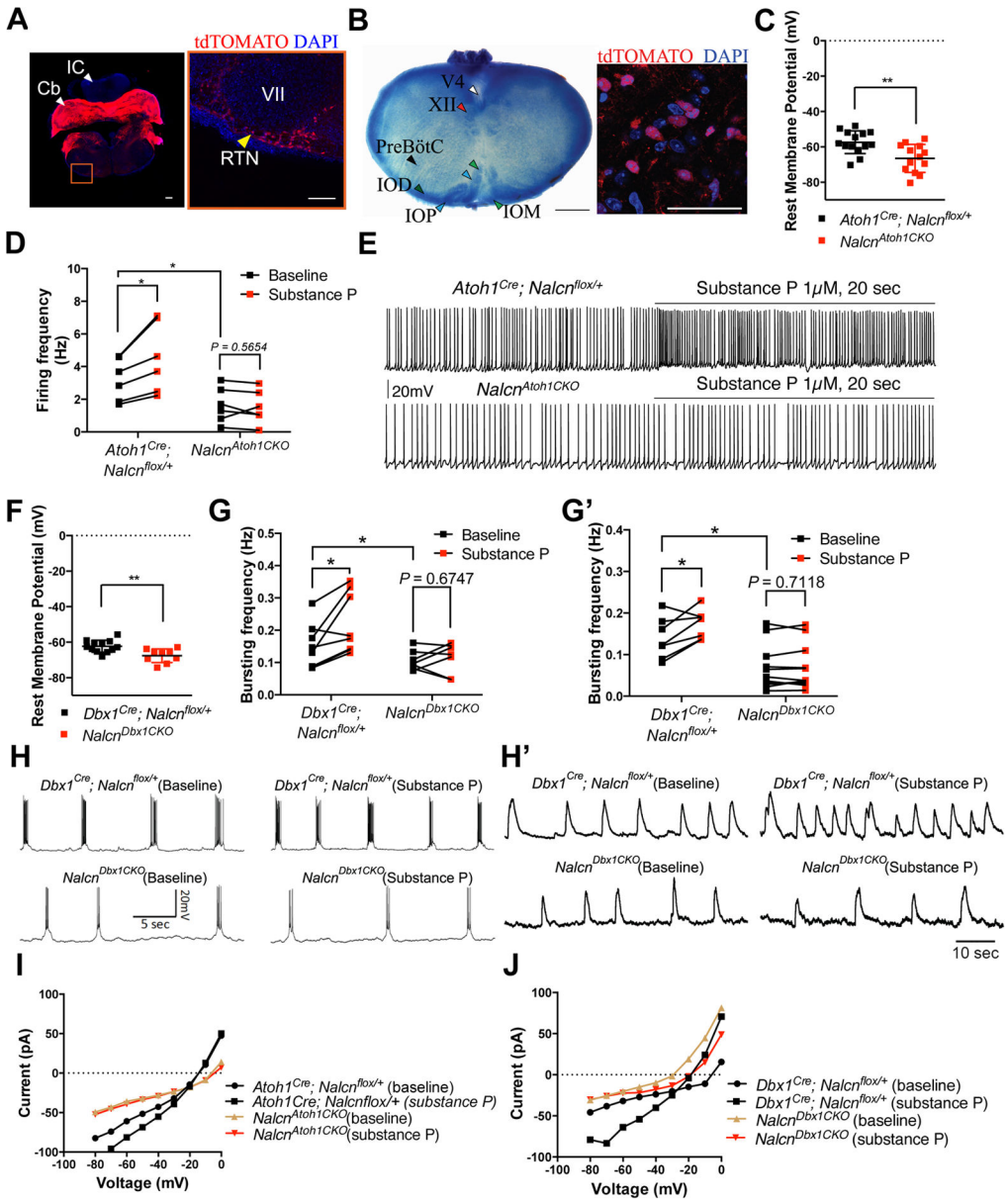

Figure 2. Nalcn in the RTN and preBötC establishes rhythmic activity and modulatory response to substance P

(A) Atoh1^{+} RTN neurons (yellow arrowhead) ventral to the facial nucleus (VII) were labeled with *ROSA*^{tdTOMATO} allele (red). Scale bars represent 200 (left) and 100 μm (right). Abbreviation: Cb, cerebellum; IC, Inferior colliculus

(B) *Left*: Thionin-stained brain slice containing the preBötC region. *Right*: Dbx1^{+} preBötC neurons were labeled with *ROSA*^{tdTOMATO} allele (red). Scale bars represent 500 (left) and 50 μm (right). Abbreviation: V4, fourth ventricle; XII, hypoglossal nucleus; IOD, dorsal aspect of inferior olive; IOP, principal loop of inferior olive; IOM, medial aspect of inferior olive

(C) Resting membrane potential of P0 RTN neurons from *Nalcn*^{Atoh1CKO} (n=13) and *Atoh1*^{Cre}*; NALCN*$^{flox/+}$ mice (n=14). (Independent sample t-test)

(D–E) Baseline firing frequency and modulatory response to 1 μM substance P of P0 RTN neurons from *Nalcn*^{Atoh1CKO} (n=6) and *Atoh1*^{Cre}*; NALCN*$^{flox/+}$ mice (n=6). (Paired two-way ANOVA)

(F) Resting membrane potential of P0 preBötC neurons from *Nalcn*^{Dbx1CKO} (n=9) and *Dbx1*^{Cre}*; NALCN*$^{flox/+}$ mice (n=12). (Independent sample t-test)

(G–H) Baseline firing frequency and modulatory response to substance P of P0 preBötC neurons from *Nalcn*^{Dbx1CKO} (n=7) and *Dbx1*^{cre}*; NALCN*$^{flox/+}$ mice (n=8). (Paired two-way ANOVA)

(G′–H′) Baseline respiratory output and modulatory response to substance P from *Nalcn*^{Dbx1CKO} (n=11) and *Dbx1*^{cre}*; NALCN*$^{flox/+}$ mice (n=8). (Paired two-way ANOVA)

(I) *I–V* relationship of the RTN neurons at baseline and effects of 1 μM substance P from *Nalcn*^{Atoh1CKO} (n=11) and *Atoh1*^{Cre}*; NALCN*$^{flox/+}$ mice (n=4).

(J) *I–V* relationship of the preBötC neurons in baseline and effects of 1 μM substance P from *Nalcn*^{Dbx1CKO} (n=6) and *Dbx1*^{Cre}*; NALCN*$^{flox/+}$ mice (n=6).

Mean ± SD, *: $P < 0.05$; **: $P < 0.01$

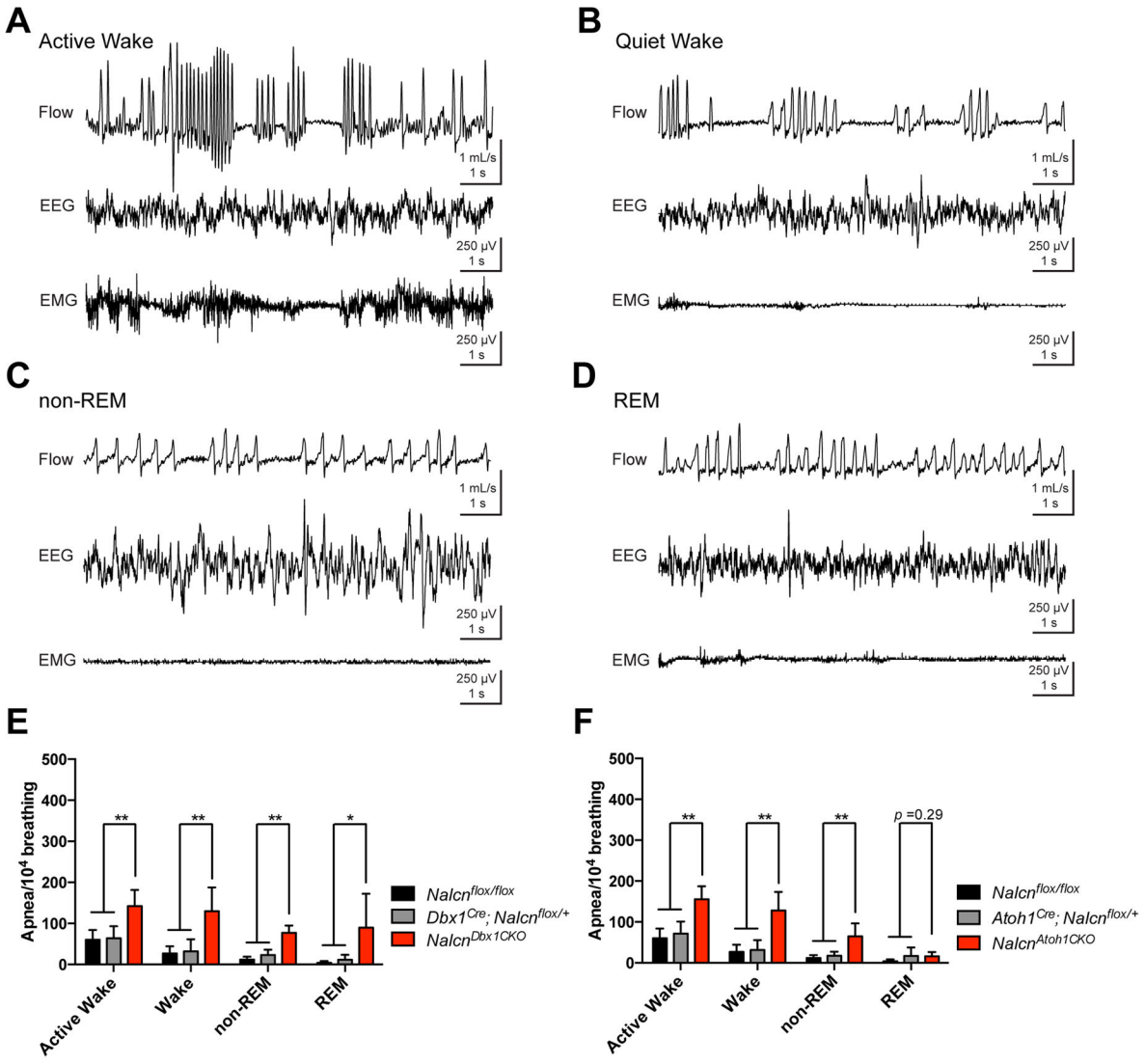

Figure 3. Loss of *Nalcn* in the preBötC or Atoh1^{+} lineage leads to apneas during both awake and sleep states

(A–B) EEG, EMG, and breathing traces of *Nalcn*^{Dbx1CKO} mice from active wake, quiet wake, non-REM, and REM stages.

(C–F) UWBP of 8–12 weeks old *Nalcn*$^{flox/flox}$ (n=5), *Atoh1*^{Cre}*; NALCN*$^{flox/+}$ (n=5), *Nalcn*^{Atoh1CKO} (n=5), *Dbx1*^{Cre}*; NALCN*$^{flox/+}$ (n=5), and *Nalcn*^{Dbx1CKO} (n=5) mice in active wake, quiet wake, non-REM, and REM stages.

One-way ANOVA, mean ± SD, *: $P < 0.05$; **: $P < 0.01$

Table 1

Neonatal lethality in different *Nalcn* conditional knockout mice.

Cre line	Target	Animal number			Chi-square test p-value	Homozygous CKO lethality (%)
		$Nalcn^{flox/+}$ $Nalcn^{flox/flox}$	Heterozygous	Homozygous		
$Nestin^{Cre}$	CNS	107	51	43	0.4777	100
$Vglut2^{Cre}$	Glutamatergic neurons	74	21	29	0.0585	100
$Viaat^{Cre}$	GABAergic neurons	131	54	38	0.0105	13.2
$Chat^{Cre}$	Cholinergic neurons	55	35	22	0.2172	0
$Pet1^{Cre}$	Serotonergic neurons	43	17	20	0.7136	0
$GlyT2^{Cre}$	Glycinergic neurons	112	61	40	0.0949	0
$Atoh1^{Cre}$	RTN	22	12	12	0.9575	0
$Phox2b^{Cre}$	RTN	74	36	35	0.9628	0
$Dbx1^{Cre}$	PreBötC	60	35	43	0.1944	32.6
$En1^{Cre}$	Rhombomere 1	76	43	42	0.7728	0

Cre line	Target	Animal number				Chi-square test p-value	$Nalcn^{Dbx1CKO}$ lethality (%)	$Nalcn^{DCKO}$ lethality (%)
		$Nalcn^{flox/flox}$	$Nalcn^{Atoh1CKO}$	$Nalcn^{Dbx1CKO}$	$Nalcn^{DCKO}$			
$Dbx1^{Cre}$ $Atoh1^{Cre}$	PreBötC RTN	18	12	17	20	0.5571	29.4	30.0

Abbreviation: CNS, central nervous system; RTN, retrotrapezoid nucleus; preBötC, preBötzinger Complex